

Supplementary information

Direct observation of protein structural transitions through entire amyloid aggregation processes in water using 2D-IR spectroscopy

So Yeon Chun,^{‡a,b} Myung Kook Son,^{‡b,c,d} Chae Ri Park,^{b,c,d} Chaiho Lim,^{a,b} Hugh I. Kim,^{*b,c,d} Kyungwon Kwak,^{*a,b} and Minhaeng Cho^{*a,b}

^a Center for Molecular Spectroscopy and Dynamics, Institute for Basic Science (IBS), Seoul 02841, Republic of Korea

^b Department of Chemistry, Korea University, Seoul 02841, Republic of Korea

^c Center for Proteogenome Research, Korea University, Seoul 02841, Republic of Korea

^d Single Cell Analysis Laboratory, Korea University, Seoul 02841, Republic of Korea

Experimental Procedures

Results and Discussion

Supplementary Note I . Kinetics of insulin fibrillation at various conditions (concentrations, buffer, pH)

Figure S1. Incubation time-dependent CD spectra of INS in H₂O and D₂O

Table S1. Relative populations of secondary structure elements of INS in H₂O

Table S2. Relative populations of secondary structure elements of INS in D₂O

Figure S2. Fibrillation kinetics of INS in various conditions (concentrations, buffer)

Figure S3. Fibrillation kinetics of INS-H₂O and INS-D₂O at experimentally measured pH value of 1.7, 2.1, and 2.5

Figure S4. Fibrillation kinetics of INS-H₂O at pH 1.7 and 2.1

Table S3. Approximate lag time of INS-H₂O at three different pH conditions (1.7, 2.1, and 2.5)

Figure S5. Comparison of the CD spectra INS in H₂O and D₂O before fibrillation

Supplementary Note II . FT-IR spectroscopy of insulin

Figure S6. FT-IR spectra of solvent and INS

Supplementary Note III . H-D exchange of insulin in D₂O

Figure S7. FT-IR spectroscopic evidence on the H-D exchange process of INS in D₂O

Figure S8. ESI-MS and ESI-IMS spectra of INS-H₂O and INS-D₂O

Figure S9. Calibration curve using standard proteins with known CCS values obtained by IM-MS

Supplementary Note IV . 2D-IR spectroscopy of insulin

Figure S10. Incubation time-dependent FT-IR spectra of INS in H₂O and D₂O solutions

Figure S11. 2D-IR spectra of INS in H₂O at waiting times of 100, 250, and 400 fs

Figure S12. 2D-IR spectra of INS in D₂O at waiting times of 100, 250, and 400 fs

Figure S13. 2D-IR spectra of INS in D₂O before incubation

Additional Supplementary Figures and Tables

Figure S14. 2D-IR spectrum of INS in H₂O at 20 h of incubation and that in D₂O at 24 h of incubation

Figure S15. X-ray diffraction structures of INS monomer (PDB code 3E7Y)

Figure S16. MD simulated structures of INS dimers in H₂O and D₂O

Table S4. R_g and helicity values of MD simulated INS dimers

Supplementary Note V . Additional supporting information

Figure S17. Solution phase SAXS analysis of denatured INS (1 mg/mL) and χ^2 - R_g diagram obtained with CRY SOL

Figure S18. ThT assay of denatured INS in H₂O and D₂O

Figure S19. Incubation time-dependent intensities of two FT-IR bands representing α -helix and β -sheet

Additional Supplementary Figure

Figure S20. DSC thermograms of INS in H₂O and D₂O

Experimental Procedures

Sample preparation. INS, a human recombinant, was obtained from SAFC Biosciences Inc. (Lenexa, Kansas, US) and used without further purification. Deuterium oxide (99.9 atom % D), deuterium chloride solution (35 wt. % in D₂O, ≥99 atom % D), and hydrochloric acid (ACS-grade reagent, 37%) were obtained from Sigma–Aldrich. Distilled water was obtained from a water purification system (Milli-Q, Merck). Hydrochloric acid and deuterium chloride were used to set the appropriate pH and pD of the INS solutions in H₂O and D₂O to 2.1. The pD was measured using the following equation.¹

$$\text{pD} = \text{pH}^{\text{Measured in solution}} (\text{pH}^{\text{M}}) + 0.40$$

The heavy water effect on the pK_a of the side chain in the protein can affect the stability of the protein; however, this effect was considered insignificant.² To study the spectroscopy of INS samples, INS was dissolved in water (INS-H₂O) and heavy water (INS-D₂O) at a concentration of 17 mg/mL (~2.93 mM). An incubation shaker (IST-3075R, Jeio Tech) was used for fibrillation of the INS samples at an incubation temperature of 323.15 K and 25 revolutions per minute (RPM). To study the spectroscopy of INS fibrillation, INS solutions were extracted 100 μ L at regular intervals. To study the fibrillation processes of INS at 1 mg/mL (~172.2 μ M) and 2 mg/mL (~344.4 μ M) concentrations, we added INS dissolved in H₂O or D₂O (total volume of 300 μ L) to 0.3-mL borosilicate glass vials with V-shaped bottom (Wheaton, USA, Millville, NJ, cat. No. 03-410-020), incubated the solution sample at a temperature of 323.15 K. The RPM value for the incubation of 1 and 2 mg/mL INS solution was 75 and 50, respectively.

Acid buffer solution (0.1 M HCl (DCI)-KCl buffer solution with 0.1 M KCl) was prepared with 0.1 M KCl, and $\text{pH}^{\text{M}} = 1.7, 2.1,$ and 2.5 adjusted using 1 M HCl (DCI).³⁻⁵ Stock solutions of 2 mg/mL and 20 mg/mL INS were dissolved in acid buffer solution. Then, pH^{M} was adjusted to 1.7, 2.1, and 2.5 using 0.5 M HCl (DCI). For ThT fluorescence assay, stock solutions were diluted to 1 mg/mL and 17 mg/mL with acid buffer solutions at a given pH (pD), in the presence of 5 and 20 μ M thioflavin T (ThT), respectively.

Thioflavin T (ThT) fluorescence assay. Thioflavin T (ThT) was purchased from Sigma-Aldrich. The ThT fluorescence for 1, 2, and 17 mg/mL INS were measured using a fluorescence spectrometer (FluoroMate FS-2, SCINCO). To prepare for 1 and 2 mg/mL INS solutions, 5 μ L aliquots were mixed with 145 μ L of ThT solution, and fluorescence was measured (ex: 446 nm, em: 482 nm) using a fluorescence spectrometer. The INS solution of 17 mg/mL was dissolved in a 50 μ M ThT solution at a concentration of 17 μ g/mL (~2.93 μ M) (1/1000 diluted) for ThT fluorescence measurement. ThT fluorescence spectra were obtained from 3 co-added scans, and a cuvette with a path length of 1 mm was used. The ThT kinetic analysis of fibril formation in 1, 2, and 17 mg/mL INS solutions was obtained at 2, 6 hours, and 30 minutes incubation intervals, respectively.

For ThT fluorescence assay of 17 mg/mL INS in acid buffer solutions (0.1 M HCl (DCI)-KCl buffer solution with 0.1 M KCl), INS-H₂O at pH = 2.1 and INS-D₂O at pD = 2.1 were co-incubated with 20 μ M ThT at 45 °C (due to instrumental limitation of 45 °C). For pH-controlled ThT fluorescence assay of 1 mg/mL INS in acid buffer solutions, INS-H₂O and INS-D₂O at $\text{pH}^{\text{M}} = 1.7, 2.1,$ and 2.5 were co-incubated with 5 μ M ThT at 45 °C. Samples were incubated with continuous orbital shaking of 807 cpm using Corning® 96-well black polystyrene microplate (Corning 3603, Corning, New York, USA) with sealing (EASYseal sealing film, Greiner-Bio-One). The ThT fluorescence was monitored using Synergy H1 microplate reader (BioTek, Winooski, USA) with excitation and emission wavelengths of 446 and 482 nm, respectively, from the top of the plate every 30 minutes up to 40 hours for 17 mg/mL, and 70 hours for 1 mg/mL.

Circular dichroism (CD) spectroscopy. Circular dichroism (CD) spectra were measured using a circular dichroism spectrometer (J-815, JASCO). During incubation, INS solutions sampled at a concentration of 17 mg/mL (~2.93 mM) were

extracted at regular intervals and dissolved in pure solvent at a concentration of 170 $\mu\text{g}/\text{mL}$ ($\sim 29.3 \mu\text{M}$) for CD measurement. The data pitch and scanning speeds were 0.5 nm and 50 nm/min, respectively. CD spectra were obtained from 5 co-added scans, and a cuvette with a path length of 1 mm was used. The CD spectra were measured for a small amount of sample taken from the incubation vessel every hour (Figure S1a). We measured the CD spectra of three independent samples. The standard deviation of CD intensity at 208 nm is presented as an error bar in Figure S1b. The secondary structure ratio analysis of the obtained CD spectra (Tables S1 and S2) was processed using the BeStSel server⁶

Transmission electron microscopy (TEM). Incubated INS- H_2O and INS- D_2O fibrils were diluted 20-fold with pH-adjusted water (pH = 2.1) and heavy water (pD = 2.1) at 28 h. Then, the diluted fibril solution (5 μL) was transferred to a 400-mesh formvar/carbon Cu(II) grid (Electron microscopy science, USA, Hatfield, PA) and removed after 3 min. Five microliters of 0.5% w/v uranyl acetate (UA) solution was transferred to the grid and removed immediately. The grid was stained with 5 μL of 0.5% w/v UA for 3 min and then removed. Samples were dried for 4 h at room temperature. The treated grids were analyzed using a JEM-F200 (TFEG) transmission electron microscope (JEOL Ltd, Japan) at the National Center for Inter-University Research Facilities (NCIRF, Seoul, Republic of Korea).

Fourier transform infrared (FT-IR) spectroscopy. Fourier transform infrared (FT-IR) absorption spectra were measured using an FT-IR spectrometer (Frontier, PerkinElmer). For IR measurements of INS samples in H_2O and D_2O , samples were housed between two CaF_2 windows using 6 μm - and 25 μm -thick Teflon spacers, respectively. 6 and 25 μL INS solution samples were used for the FT-IR measurements with 6 μm (in H_2O) and 25 μm (in D_2O) spacers, respectively. Spectra were obtained by 9 co-added scans at a resolution of 0.2 cm^{-1} in the spectral region of 400–8000 cm^{-1} .

Two-dimensional IR (2D-IR) spectroscopy. Two-dimensional IR (2D-IR) experiments were carried out using 800 nm pulses with a duration of < 35 fs, and 6 mJ pulses were generated from a Ti:Sapphire oscillator and regenerative amplifier (Solstice Ace, Spectra-Physics) operating at 1 kHz, which were then used to produce near-infrared pulses at $\sim 1.41 \mu\text{m}$ (Signal) and $\sim 1.84 \mu\text{m}$ (Idler) by an optical parametric amplifier (OPA) system (TOPAS Prime, Spectra-Physics). With a AgGaS_2 nonlinear optical crystal, the signal and idler pulses were mixed to generate mid-infrared pulses with a pulse energy of $\sim 10.93 \mu\text{J}$, full width at half maximum (FWHM) of $\sim 240 \text{cm}^{-1}$, duration time of ~ 61.1 fs, and center wavenumber of $\sim 1660 \text{cm}^{-1}$. This pulse was split into three parallel polarized pulses (\mathbf{k}_1 , \mathbf{k}_2 , \mathbf{k}_3) and focused on the sample in a box-CARS geometry to generate the transient grating signal. A local oscillator pulse was used to enhance the transient grating signal intensity by heterodyne detection. A heterodyned photon echo signal was detected using a monochromator (iHR320, HORIBA) and a 64-element mercury cadmium telluride (MCT) array detector. For the 2D-IR measurements of the INS samples, we used the same sample conditions as those used for linear IR spectroscopy, and the 2D-IR spectra were obtained by a single scan at a resolution of $\sim 2 \text{cm}^{-1}$. To obtain a reference signal for phasing of the 2D-IR signal, we also measured the IR pump-probe spectra of the INS solution through 9 co-added scans.

Small-angle X-ray scattering (SAXS). The SAXS experiments were performed at the 4C SAXS II beamline of the Pohang Accelerator Laboratory (PAL). The sample-to-detector distance was set to 2 m, and all experiments were performed at 20 $^\circ\text{C}$. Stock solutions of 6 mg/mL ($\sim 1033 \mu\text{M}$) INS in water and heavy water were prepared and then diluted to 2 mg/mL ($\sim 344.4 \mu\text{M}$). The SAXS profiles for 50 μL solution were measured 10 times for 10 s, and the average radii of gyration of INS- H_2O and INS- D_2O were estimated by performing the Guinier analysis with the following equation:

$$\ln(I(q)) = \ln(I_0) - \left(\frac{R_g^2}{3}\right)q^2$$

where q is the scattering vector and $I(q)$ is the scattering intensity of q .

Molecular dynamics (MD) simulation. Before the MD simulation, missing residue 30 (THR) of the B chain was added using UCSF Chimera. Pools of simulated INS monomer and dimer structures were generated through 2 ns simulated annealing of the INS X-ray diffraction structure (PDB 3E7Y) using GROMACS 2020.4.⁷⁻⁹ The annealing temperatures of the monomers were 300, 350, 400, 450, 500, 550, and 600 K, and those of the dimers were 300, 350, 400, and 400 K with the OPLS-AA/L all-atom forcefield with the SPC/E water model and SPCE/HW heavy water model.¹⁰ 14,000 monomer structures and 8,000 dimer structures a totaling 22,000 structures were used as the theoretical conformation pool. Theoretically calculated SAXS profiles were compared with experimentally measured SAXS profiles by using CRY SOL software (EMBL Hamburg).¹¹ For the monomer/dimer ratio calculation, OLIGOMER software (EMBL Hamburg) was used. In total, five sets composed of 4 monomer conformations and 4 dimer conformations were selected from the conformation pools for subsequent analyses.

Differential scanning Calorimetry (DSC). DSC thermodynamic analysis was performed using a Nano DSC (TA Instruments) at the IFEZ Bio Analysis Center (Republic of Korea). The concentration of INS was 5 mg/mL. The temperature range was from 20 to 100 °C with a scan rate of 1 °C/min. The pH-adjusted water and heavy water solvent scans were subtracted from each sample scan. Calculations of enthalpy (ΔH_u), entropy (ΔS_u), Gibbs free energy (ΔG_u), and thermal transition temperature (T_0) were obtained using NanoAnalyze software (TA Instruments).

Results and Discussion

Supplementary Note I . Kinetics of insulin fibrillation at various conditions (concentrations, buffer, pH)

Circular dichroism spectroscopy of insulin. Figure S1a shows the CD spectra of INS in H₂O and D₂O during the fibrillation process. Initially, the spectral line shapes of the CD spectra exhibit the typical CD spectral pattern of α -helix, i.e., a strong positive band at 196 nm and two negative bands at 208 and 222 nm.¹² Their intensities decrease as the incubation time increases, which indicates the increases of the random coil population.¹³ Eventually, the CD spectra at a long incubation time (20 h for H₂O solution and 24 h for D₂O solution) show a positive band at 200 nm and a negative band at 220 nm, which is the characteristic feature of β -sheet proteins. Since the conformational transition of INS from α -helix to β -sheet is directly related to the INS fibrillation, we monitored the CD intensity at 208 nm, where the CD signature of α -helix minimally overlaps with the CD band of typical β -sheet, and plot them in Figure S1b. To confirm the reproducibility of this INS aggregation process, we measured the CD spectra of three different samples and considered the average spectrum. The standard deviations of the CD intensities at 208 nm are shown in Figure S1b. In addition, using the BeStSel program and from the measured CD spectra in Figure S1a, we estimated the relative populations of various secondary structure elements, e.g., α -helix, β -sheet, and random coil, of INS in H₂O and D₂O (Figure 1c, Tables S1 and S2).

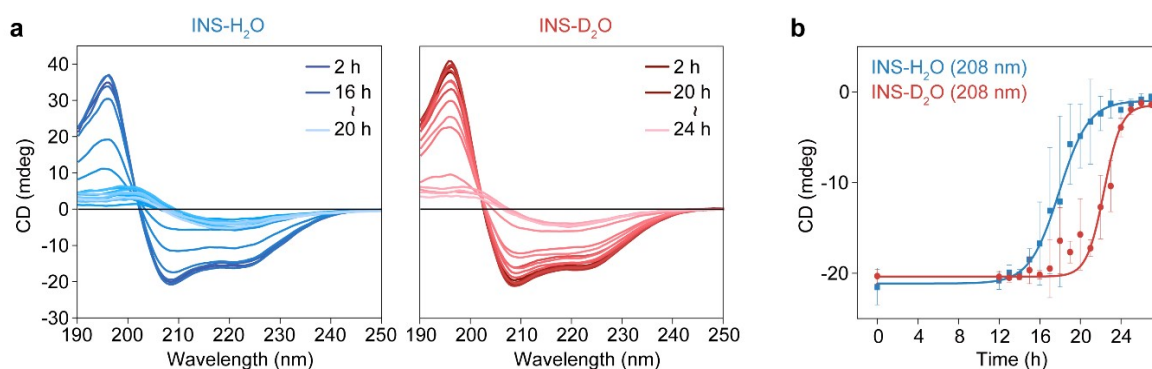


Figure S1 (a) CD spectra of INS-H₂O (left) and INS-D₂O (right) obtained every 1 h during incubation. (b) The CD intensities at 208 nm, which reflect the relative population of α -helix, are plotted with respect to the incubation time.

Table S1 Relative populations of three representative secondary structure elements (β -sheet, α -helix, and random coil) of INS in H₂O. We used our experimentally measured CD spectra (Figure S1a) and BeStSel server.

Time (h)	β -sheet (%)	α -helix (%)	Random-coil (%)
0	36	64	0
12	36.8	63.2	0
13	32.8	67.2	0
14	42.5	57.5	0
15	25	75	0
16	12	53.3	34.7
17	58.3	0	41.8
18	58.3	0	41.8
19	57.1	2.2	40.7
20	65.4	0	34.7
21	78	0	22
22	74	0	26
23	77	0	22.9
24	60.9	0	39.1
25	61.6	0	38.4
26	81.6	0	18.4
27	62.4	0	37.6
28	58	0	42

Table S2 Relative populations of three representative secondary structure elements (β -sheet, α -helix, and random coil) of INS in D₂O. We used our experimentally measured CD spectra (Figure S1a) and BeStSel server.

Time (h)	β -sheet (%)	α -helix (%)	Random-coil (%)
0	35.5	64.5	0
12	34.6	65.4	0
13	32.9	67.1	0
14	34.9	65.1	0
15	32.8	67.2	0
16	34.8	65.2	0
17	34.5	65.5	0
18	42.3	57.7	0
19	39	61	0
20	42.4	57.6	0
21	47.2	52.8	0
22	30	70	0
23	40.2	59.8	0
24	24.8	42.5	32.7
25	72.5	7.4	20
26	77.3	4.2	18.5
27	72.9	0	27.1
28	59.9	0	40.1

ThT fluorescence assay of insulin fibrillation at various concentrations and buffer conditions. We compared the kinetics of INS fibrillation at a high INS concentration of 17 mg/mL using H₂O at pH = 2.1 and D₂O at pD = 2.1 (Figure 1a) with those using acidic buffer (Figure S2a). We confirmed that the fibrillations in 17 mg/mL INS solutions occur slowly in D₂O, irrespective of the acidic buffer. The half times of fibrillation in H₂O and D₂O were 22.9 and 27.9 h, respectively (Figure S2e). In addition, we carried out ThT fluorescence assay of low-concentration INS solutions (1 and 2 mg/mL INS-H₂O (D₂O) at pH (pD) = 2.1), which was used for structural dynamics and kinetics control studies. Quantitatively similar results were obtained even at low INS concentrations with or without buffer, which shows delayed fibrillations in D₂O (Figures S2b, S2c, S2d, and S2e). The TEM images of 1 mg/mL INS-H₂O and INS-D₂O at 32 h indicate that the morphology of INS fibers formed in H₂O is similar to that in D₂O (Figure S2f).

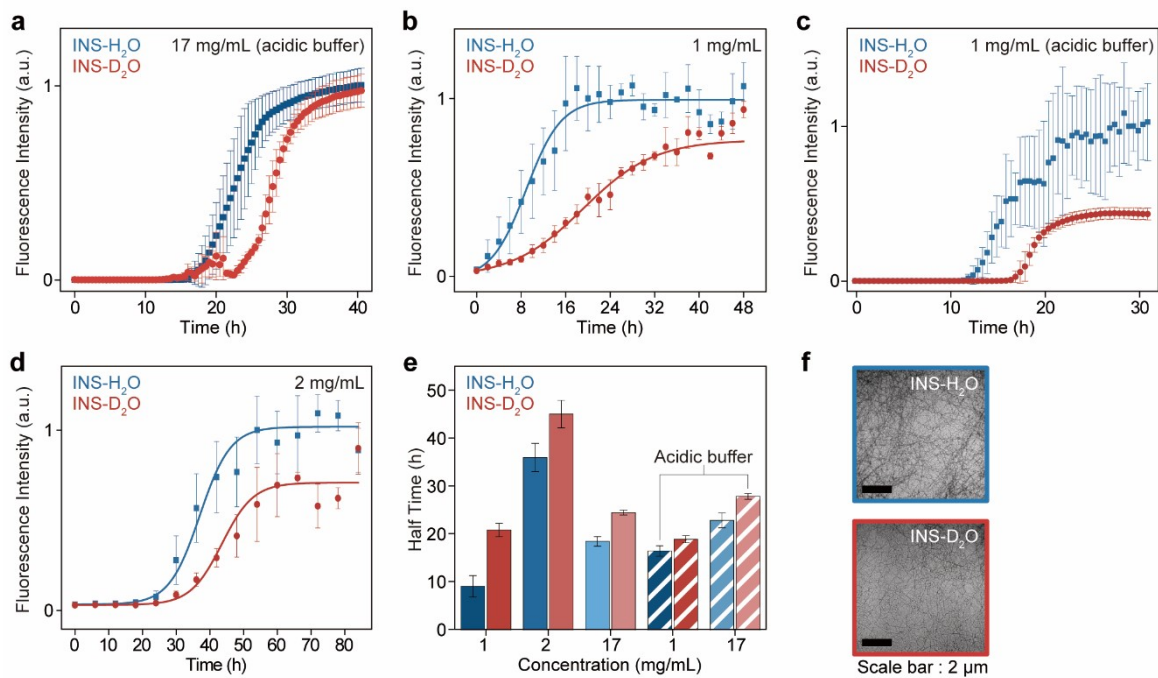


Figure S2 Fibrillation process kinetic analysis of INS at 17 mg/mL in HCl (DCI)-KCl buffer solution (a), 1mg/mL in H₂O (D₂O) (b), 1 mg/mL in HCl (DCI)-KCl buffer (c), 2 mg/mL in H₂O (D₂O) (d) at pH (pD) = 2.1. The intensities of ThT fluorescence at 490 nm are plotted with the incubation time. (e) Half time of ThT fluorescence assay for each concentration (9.1, 36, and 18.5 h for 1, 2, and 17 mg/mL INS-H₂O, respectively. 20.9, 45, and 24.5 h for 1, 2, and 17 mg/mL INS-D₂O, respectively.) (f) TEM images of 1 mg/mL INS-H₂O and INS-D₂O obtained at an incubation time of 32 h.

pH-dependence of fibrillation lag time. We found that, regardless of INS concentrations, the INS fibrillation process in D₂O at pD = 2.1 is slower than that in H₂O at pH = 2.1, where we used the following equation, $pD = pH^M + 0.40$, to convert the experimentally measured pH (pH^M) value to pD.¹ However, quite a few previous studies assumed that $pD = pH^M$. Thus, using the same assumption ($pD = pH^M$), we also examined the INS fibrillation kinetics. Specifically, we considered three different incubation conditions at $pH^M = 1.7, 2.1,$ and 2.5 . The ThT fluorescence assays of 1 mg/mL INS-H₂O and INS-D₂O at three different pH^M conditions (using acid buffer) are compared with one another in Figure S3. It is notable that the difference in the half time ($t_{1/2}$) of the INS fibrillation in H₂O and D₂O increased as pH^M decreased. Although the aggregation kinetics is pH-sensitive, both results (Figure 1a and S3e) clearly indicate that the INS fibrillation occurs slowly in D₂O, compared to that in H₂O.

To find an appropriate pH (pD) for studying the fibrillation process of INS at a high concentration of 17 mg/mL, we carried out CD studies of INS fibrillations for varying pH^M 's. The CD intensity of INS-H₂O at a protein concentration of 17 mg/mL and at a wavelength of 208 nm is plotted with respect to incubation time in Figure S4 (Table S3). Since the fibrillation process with a lag time of 15 h or longer are suitable for kinetics studies using ThT fluorescence, CD, and IR spectroscopy, we used INS solutions at $pH(pD) = 2.1$ for subsequent 2D-IR spectroscopic investigations.

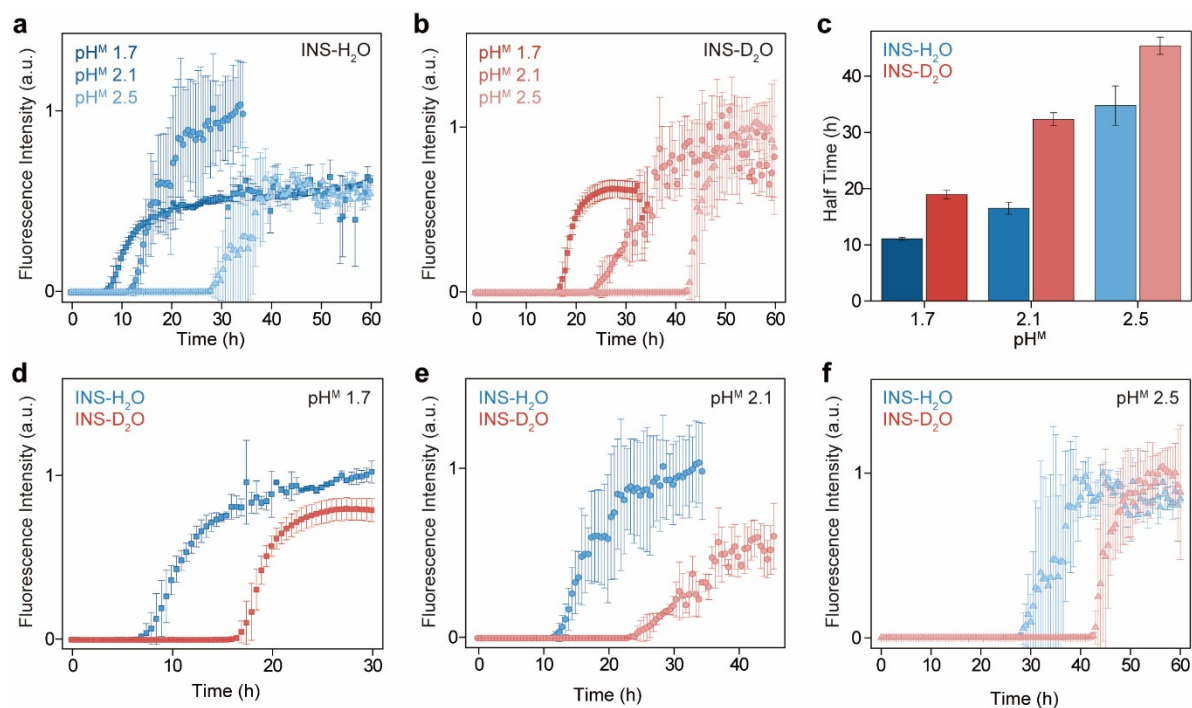


Figure S3 The ThT fluorescence assay of INS-H₂O (a) and INS-D₂O (b) with different pH^M conditions (1.7, 2.1, and 2.5). (c) Half time of ThT fluorescence assay for each pH^M (11, 16.5 and 34.8 h for INS-H₂O $pH^M = 1.7, 2.1$ and 2.5 respectively. 19, 32.4 and 45.4 h for INS-D₂O $pH^M = 1.7, 2.1$ and 2.5 respectively.). (d), (e), (f) Comparison of ThT fluorescence assays assuming $pD = pH^M$.

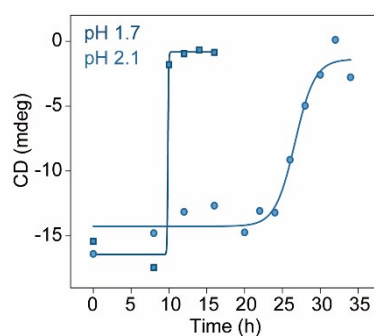


Figure S4 The CD intensity of 17 mg/mL concentration INS-H₂O at 208 nm is plotted with incubation time, where pH is either 1.7 (black) or 2.1 (blue). INS-H₂O at pH 2.5 did not form fibrils until 36 h of incubation, and the plot is not shown.

Table S3 Approximate lag times of INS-H₂O at three different pH conditions (1.7, 2.1, and 2.5), which were estimated from the analyses of incubation time-dependent CD spectra.

	pD	pH ^M	Lag time (h)
INS-H ₂ O		1.7	<10
		2.1	16~20
		2.5	>34
INS-D ₂ O	2.1	1.7	>20

Deuterium isotope effect on the CD spectrum of insulin in D₂O. Figure S5 shows the CD spectra of INS in H₂O and D₂O at 0 h of incubation. The positive CD peaks of INS-D₂O at 196 and 210-220 nm are slightly stronger than that of INS-H₂O. The experimental results suggest that the propensity of INS forming α -helix in D₂O is a bit higher than that in H₂O, which is consistent with Chellgren and Creamer's work.¹⁴ One can explain the present experimental results as follows. Due to the slightly increased H(D)-bond strength in D₂O, the average number of D-bonds per D₂O molecule in D₂O is slightly larger than that of H-bonds per H₂O molecule in H₂O. Therefore, the entropic cost of dissolving a solute molecule, including protein and other biomolecules, in D₂O is higher than H₂O.^{15, 16} This difference in solvation thermodynamics makes the interaction between hydrophobic residues in the core region of INS dissolved in D₂O stronger than that in H₂O.^{14, 17}

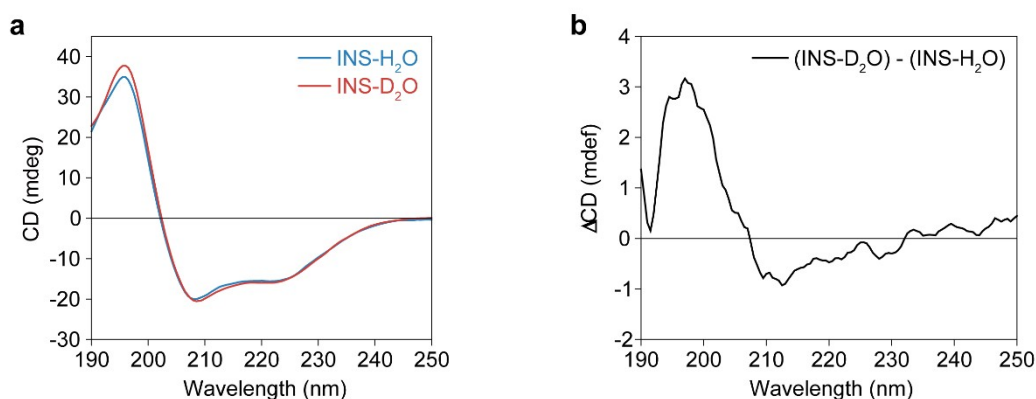


Figure S5 (a) The CD spectra of INS in H₂O and D₂O at 0 h of incubation. (b) The difference spectrum, defined as CD(INS-D₂O) – CD(INS-H₂O) is shown in this figure.

Supplementary Note II. FT-IR spectroscopy of insulin

Spectral congestion and solvent background correction. The FT-IR spectra of H₂O, INS-H₂O, D₂O, and INS-D₂O are shown in Figure S6. The spectrum associated with the bending mode of D₂O (δ_{D-O-D} , 1560 cm⁻¹) is clearly distinguishable in the frequency domain because the amide I band ($\nu_{C=O}$), mainly the C=O stretching mode of the peptide bond, appears at 1600-1700 cm⁻¹ (Figure S6b). However, the H-O-H bend IR spectrum of H₂O (δ_{H-O-H} , 1650 cm⁻¹) substantially overlaps with the amide I band (Figure S6a). Therefore, it has been inevitable for IR spectroscopists to use D₂O as a solvent for proteins. However, it is not entirely impossible to subtract the solvent FT-IR spectrum from that of protein solutions, as has been demonstrated here (see Figure 2a). Such solvent background correction was achieved with the following two-step procedure. First, the lowest absorbance value, constant offset, of each IR spectrum of INS-H₂O and INS-D₂O is subtracted from the corresponding raw spectrum. Second, for the pure H₂O and INS-H₂O spectra, the combination bands of water bending mode and intermolecular librational mode ($\delta_{H-O-H} + \nu_{libr}$) of H₂O at 2125 cm⁻¹, which does not overlap with the amide I band of INS, are normalized. Then, the two spectra are subtracted from each other to obtain the amide I IR spectrum of INS in H₂O. For the pure D₂O and INS-D₂O spectra, the combination bands of heavy water bending mode and OD stretch mode ($\delta_{D-O-D} + \nu_s$) of D₂O at 3840 cm⁻¹ are normalized, followed by the subtraction to obtain the amide I IR spectrum of INS in D₂O.

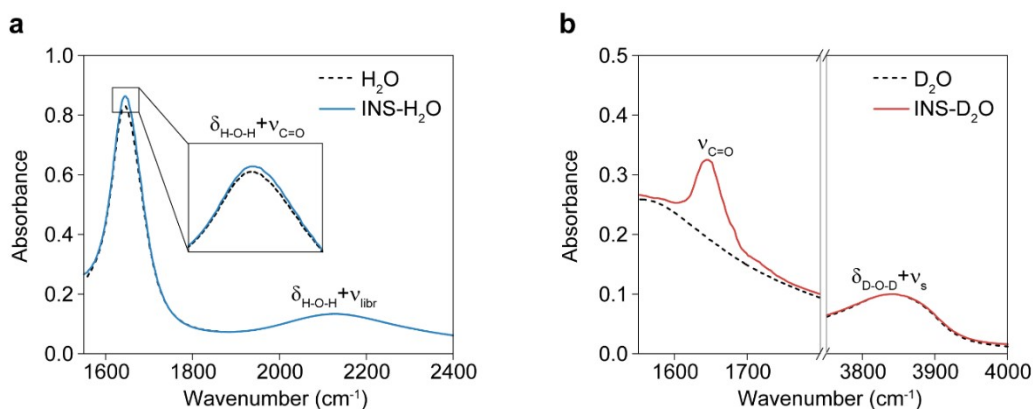


Figure S6 (a) FT-IR spectra of H₂O and INS-H₂O (17 mg/mL). (b) FT-IR spectra of D₂O and INS-D₂O (17 mg/mL).

Supplementary Note III. H-D exchange of insulin in D₂O

FT-IR spectroscopy of H-D exchange process of insulin in D₂O. When a given protein is dissolved in D₂O, all the labile protons, e.g., peptide N-H, could be replaced by deuteriums. We monitored such an H-D exchange process with FT-IR spectroscopy. The concentration of INS in D₂O was approximately 17 mg/mL. The solution temperature was maintained at 50 °C for 2 h. Figure S7 shows the FT-IR spectra of INS in D₂O at 0 and 2 h of incubation. The amide II band at around 1550 cm⁻¹, which is associated with peptide in-plane N-H bending vibration, decreases, and the amide II' band at around 1450 cm⁻¹ increases simultaneously. This is clear evidence of the H-D exchange process that is completed in approximately 2 h of incubation. Therefore, we measured both the FT-IR and 2D-IR spectra of INS-D₂O samples only after 2 h of incubation.

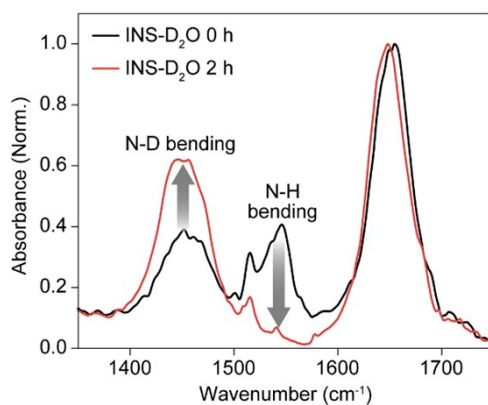


Figure S7 Solvent subtracted IR absorption spectra of INS-D₂O obtained at 0 and 2 h of incubation, showing the H-D exchange.

ESI-IM-MS analysis. The H-D exchange of insulin in D₂O was also confirmed using electrospray ionization-ion mobility-mass spectrometry (ESI-IM-MS). ESI-IM-MS experiments were performed with a Waters Synapt G2Si HDMS quadrupole time-of-flight (Q-TOF) mass spectrometer (Waters, Manchester, UK) with traveling-wave ion-mobility spectrometry (TWIMS) capability. INS-H₂O and INS-D₂O (5 μM) were sprayed into the ESI source at a flow rate of 5 μL/min. The capillary voltage was 3.0 kV, and the source temperature was 80 °C. The gas flow rates for the helium and drift cells were 180 and 90 mL/min, respectively, which provided a pressure of 4.18 mbar in the drift cell. The wave velocity and wave height were 650 m/s and 40 V, respectively. The arrival time of the target ions was converted to the collision cross-section using a previously reported protocol (Figure S9).¹⁸⁻²⁰

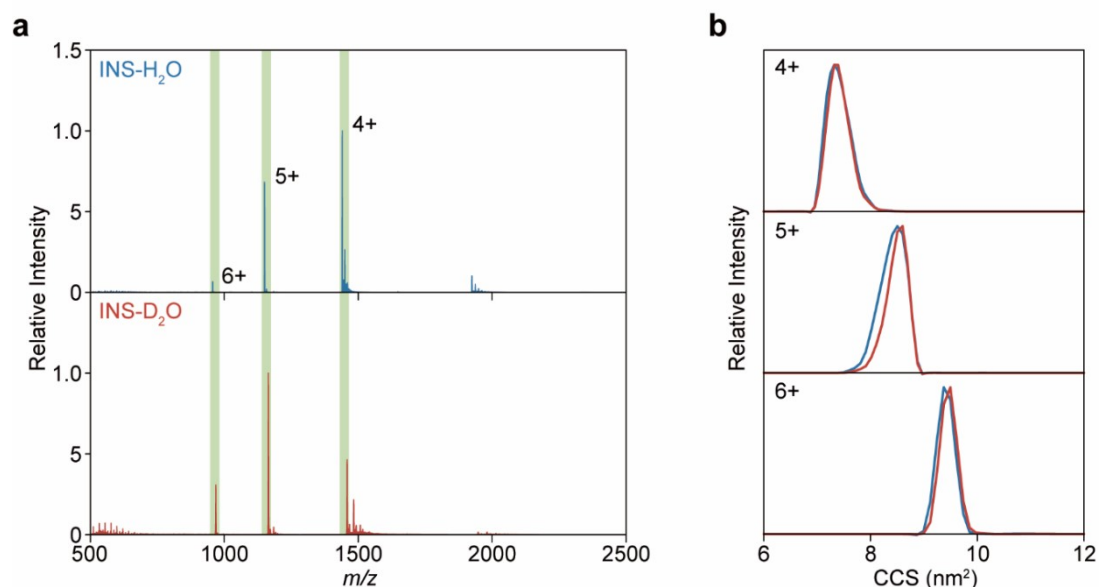


Figure S8 ESI-MS (a) and ESI-IMS spectra (b) of INS-H₂O and INS-D₂O (5 μM) obtained using a Synapt G2-Si IM-MS instrument approximately 2 hours after sampling. Due to deuteration, MS peak of +4 (m/z 1453.07), +5 (m/z 1162.46), +6 (m/z 969.05) charged states shifted to m/z 1470.67, 1176.75, 980.96 each. ESI-IMS spectra of INS-H₂O and INS-D₂O show no significant difference in the +4, +5, and +6 charged gaseous conformations after deuteration.

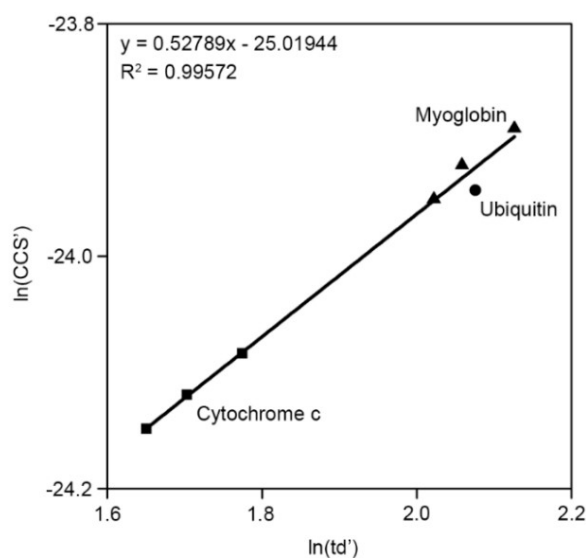


Figure S9 Calibration curve using standard proteins with known collision cross section (CCS) values obtained by IM-MS.

Supplementary Note IV. 2D-IR spectroscopy of insulin

Incubation time-dependent IR and 2D-IR spectra of insulin in H₂O and D₂O. For the 2D-IR measurements of INS in H₂O and D₂O, the solution sample was housed in a cell consisting of two CaF₂ windows separated by either 6 (INS-H₂O) or 25 (INS-D₂O) μm-thick Teflon spacer. The IR spectra after subtracting solvent spectra from the measured raw IR spectra are shown in Figure S10. When using a 6 μm-thick Teflon spacer, the total absorbance of the amide I mode of INS and H-O-H bending mode of H₂O (~1650 cm⁻¹) was found to be larger than 0.8 OD (Figure S6a). If the optical density of a given sample is large, due to the attenuation of incoming laser pulses and the self-absorption of the emitted 2D-IR field by the sample, the measured 2D-IR spectrum could be distorted. However, we didn't use a thinner sample cell because the absorbance of INS after subtracting the background solvent H₂O is very small (<0.05 OD at 2 h of incubation, Figure S10a). Although the total absorbance at ~1650 cm⁻¹, which is the sum of the absorbances of both water bending mode and INS amide I mode, was larger than 0.8 OD, we found no significant distortion in the measured 2D-IR spectra (Figure 2b and Figure S11).²¹ It is well-known that the sample with high OD could affect the estimations of FWHMs of both diagonal and cross peaks and the 2D-IR lineshapes. Fortunately, such effects are insignificant in the present qualitative analyses of protein's secondary structures from the measured 2D-IR spectra. Figures S11 and S12 show the 2D-IR spectra at $T_w = 250$ fs after subtracting the solvent background signals from H₂O or D₂O, which show no notable spectral distortions.

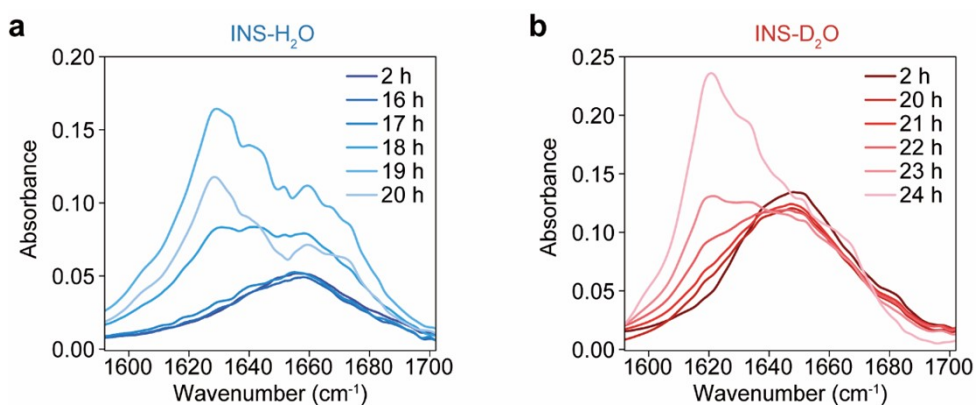


Figure S10 Incubation time-dependent IR absorption spectra of INS-H₂O (a) and INS-D₂O (b).

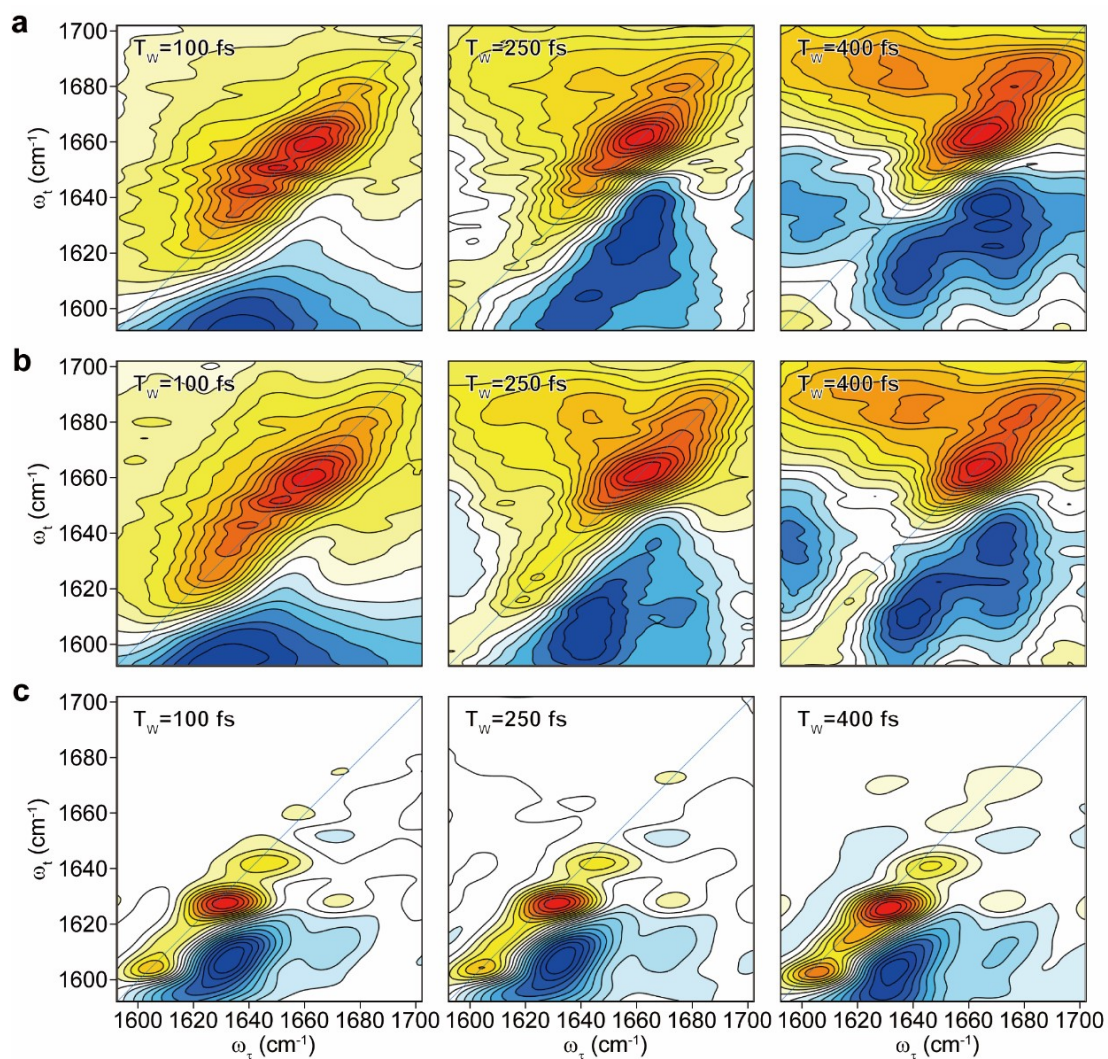


Figure S11 The 2D-IR spectra of INS-H₂O at waiting times of 100, 250, and 400 fs. Here, the incubation times are 2 h (a), 16 h (b), and 20 h (c).

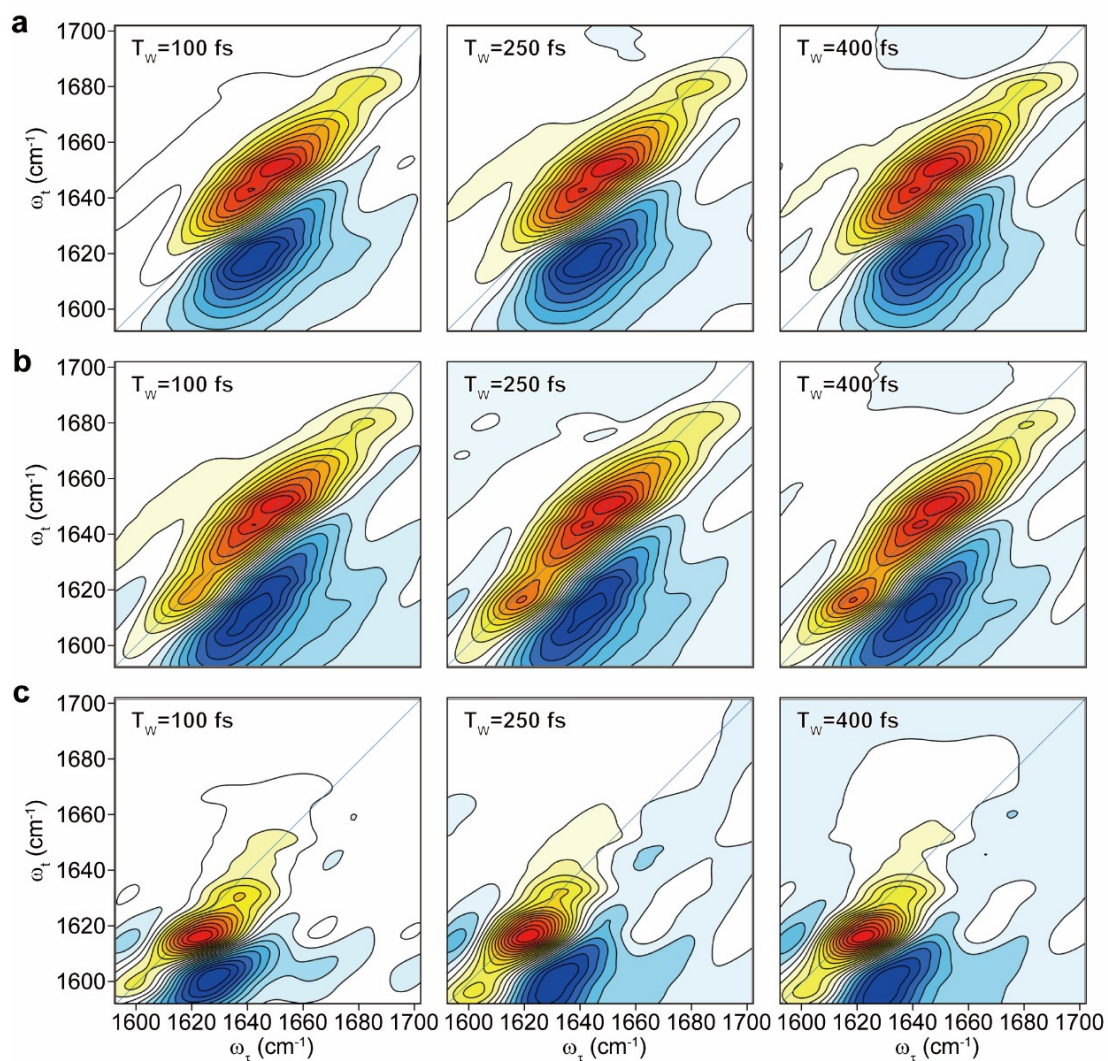


Figure S12 The 2D-IR spectra of INS-D₂O at waiting times of 100, 250, and 400 fs. The incubation times are 2 h (a), 20 h (b), and 24 h (c).

Insulin structure in D₂O before incubation. The 2D-IR and diagonal slice spectra were obtained and examined to confirm that incubating the INS-D₂O solution at 50 °C and 25 rpm for 2 h affects the initial structure of INS in D₂O. As shown in Figure S13, the 2D-IR spectrum of INS-D₂O at 0 h of incubation shows that the dominant feature at ~1656 cm⁻¹ represents the α -helix. Furthermore, two additional shoulder peaks at ~1640 and ~1688 cm⁻¹ can be assigned to the delocalized ν_{\perp} and ν_{\parallel} amide I modes of β -sheet, respectively. The spectral lineshapes of both 2D-IR and diagonal slice spectra of INS-D₂O indicate that the incubation for 2 h does not affect the initial INS structure in D₂O. In other words, the INS dimer structure in D₂O is intrinsically due to the influence of the solvent surrounding the protein, not due to the H-D exchange process.

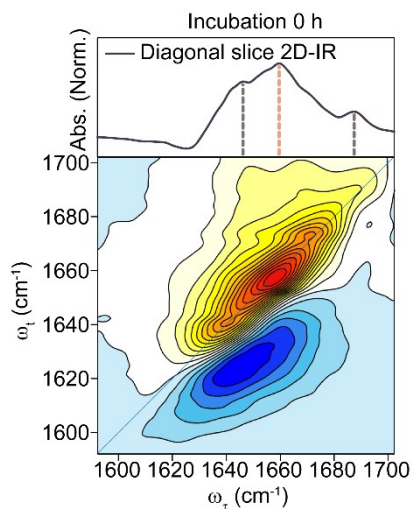


Figure S13 Diagonal slice (top) and 2D-IR spectra (bottom) of INS-D₂O obtained before incubation.

Additional Supplementary Figures and Table

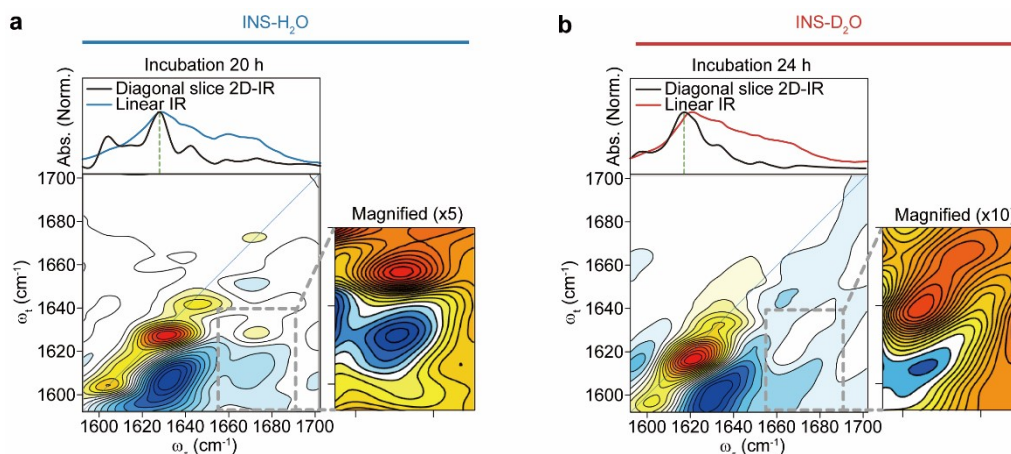


Figure S14 2D-IR spectra of INS-H₂O (~20 h) (a) and INS-D₂O (~24 h) (b) after fibrillation. The 2D-IR spectra exhibit weak high-frequency diagonal peaks and cross-peaks at ω_t of ~ 1673 cm⁻¹ and ~ 1665 cm⁻¹ in H₂O and D₂O, respectively, which are the characteristic features of the anti-parallel β-sheet structure in fibrils.

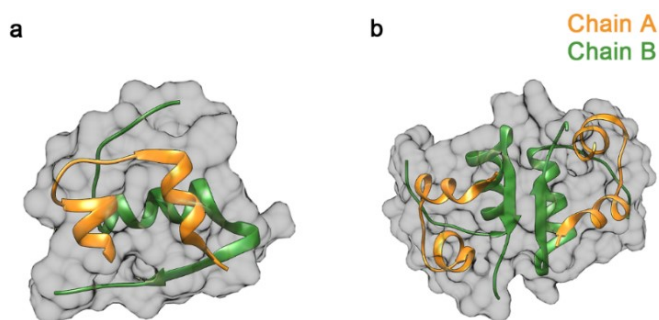


Figure S15 Human INS X-ray diffraction structures (PDB code 3E7Y) of monomer (a) and dimer (b).

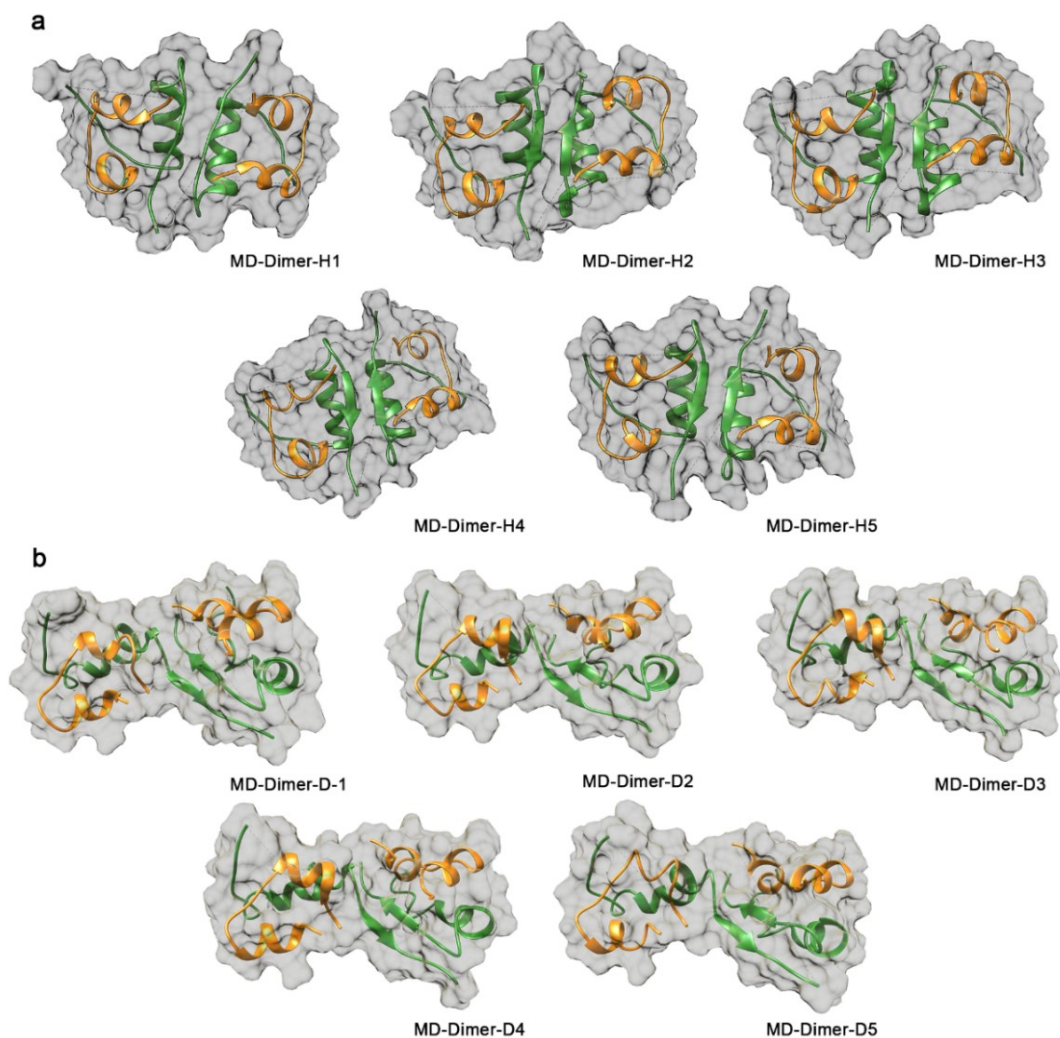


Figure S16 MD simulated structures of INS dimer obtained with MD-simulation. (a), (b) Structures of INS dimers in H₂O and D₂O (PDB code 3E7Y) with the least χ^2 values from CRY SOL results (Figure 4d). Although these candidate structures are reasonable, we need to carry out further MD simulations.

Table S4 R_g and helicity values of MD simulated INS dimers with least χ^2 values from CRY SOL results (Figure 4d).

		MD-1	MD-2	MD-3	MD-4	MD-5
H ₂ O	R_g (Å)	13.52	13.93	13.53	13.89	13.55
	Helicity (%)	47	39.2	45	48	48
D ₂ O	R_g (Å)	14.21	14.39	14.5	14.32	14.54
	Helicity (%)	47	33	33	38	42

Supplementary Note V. Additional supporting information

SAXS analyses of fully denatured insulins in H₂O and D₂O. From the ThT fluorescence assay, CD spectroscopy, and FT-IR spectroscopy of INS in H₂O and D₂O, we found that the fibrillation of INS is slower in D₂O than in H₂O. If the overall fibrillation process is diffusion-controlled, this experimental observation can be easily understood by noting that the viscosity of D₂O is larger than that of H₂O. To examine this effect originating from distinct viscosities of H₂O and D₂O on the fibrillation kinetics of INS, we investigated the fibrillation processes of fully denatured INS, instead of native INS, in H₂O and D₂O. Sodium dodecyl sulfate (SDS 50 μ M) was used for the denaturation of INS (1 mg/mL). The initial structures of native INS and denatured INS were investigated using SAXS. The results from the corresponding Guinier (Figure S17a) and Kratky analyses (Figure S17b) of the measured SAXS profiles indicate that the INS proteins are fully denatured by SDS. Note that the radius of gyration (R_g) of INS in H₂O slightly increases from 12.51 \pm 0.96 \AA for native INS to 13.79 \pm 0.88 \AA for denatured INS. Similarly, that of INS in D₂O increases from 12.39 \pm 0.92 \AA for native INS to 13.17 \pm 0.96 \AA for denatured INS. A pool of denatured INS monomer structures was generated through 2 ns simulated annealing MD simulations of INS, where its initial conformation is from the X-ray diffraction structure (PDB 3E7Y). Here, we used the GROMACS 2020.4 program. Annealing temperatures for monomers were 300, 350, 400, 450, 500, 550, 600, 700, 800, 900, and 1000 K with OPLS-AA/L all-atom forcefield with SPC/E model for H₂O and SPCE/HW for D₂O.^{10 10 10 10 10 10 7 7 7} In total, 20,000 structures were considered as a theoretical conformation pool for CRY SOL analysis.

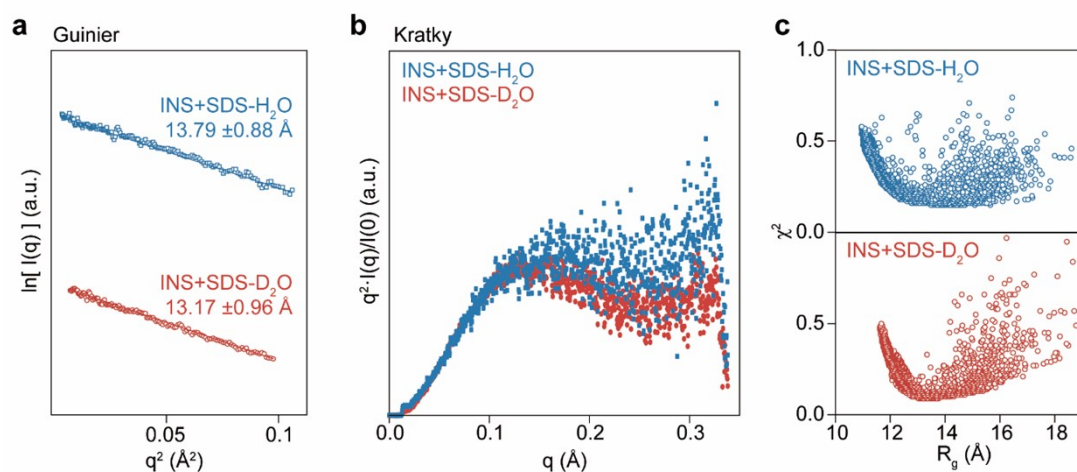


Figure S17 Solution phase SAXS analysis of denatured INS (1 mg/mL) and theoretical structures of INS obtained with MD simulation. (a) Guinier plot obtained from short q range of scattering profile. (b) Normalized Kratky analysis of insulin. (c) χ^2 - R_g diagram of INS+SDS-H₂O and INS+SDS-D₂O from the MD-simulated 20,000 conformers, obtained with CRY SOL.

ThT fluorescence assays of fully denatured insulins in H₂O and D₂O. The 1 mg/mL solutions of INS-H₂O at pH = 2.1 and INS-D₂O at pD = 2.1 with 50 μ M SDS and 20 μ M ThT were incubated at 45 °C with continuous orbital shaking of 807 cpm using Corning® 96-well black polystyrene microplate (Corning 3603, Corning, New York, USA) with sealing (EASYseal sealing film, Greiner-Bio-One). The fibrillation kinetics of denatured INS at high concentrations (17 mg/mL) could not be observed due to the rapid structure conversion to aggregates. The ThT fluorescence was monitored using Synergy H1 microplate reader (BioTek, Winooski, USA) with excitation and emission wavelengths of 446 and 482 nm, respectively, from the top of the plate every 2 hours up to 80 hours (Figure S18). Note that the fibrillation of native, not denatured, INS appears to be slower in D₂O than H₂O (Figure 1a). Therefore, if the delayed fibrillation kinetics in D₂O as compared to that in H₂O is strictly from the viscosity effect, we would expect to observe an equally slow fibrillation process of denatured INS in D₂O. However, even if the initial structures of INS are fully denatured, distinct fibrillation kinetics are no longer observed (Figure S18). This result strongly indicates that the fibrillation kinetics of the INS are predominantly affected by structural transition rates rather than diffusion rates.

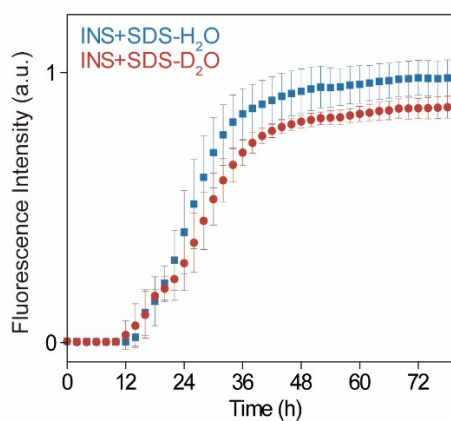


Figure S18 ThT assay comparison of denatured INS (1 mg/mL) using SDS (50 μ M) in H₂O and D₂O.

Independence of initial insulin denaturation process on protein-protein collision. To gain more information on the rate-determining step (denaturation-controlled versus diffusion-controlled) during the INS fibrillation, we carefully analyzed the FT-IR spectra of INS in H₂O and D₂O in Figure 2a. We could fit them, considering two distinct peaks A (~1658 cm⁻¹ in H₂O and ~1649 cm⁻¹ in D₂O) and B (~1629 cm⁻¹ in H₂O and ~1620 cm⁻¹ in D₂O). Since the characteristic peaks of α -helix and random coil structures appear at 1640~1660 cm⁻¹,^{13, 22, 23} the incubation time-dependent change of the peak A intensity provides information on the conformational transition of monomeric or dimeric INS by denaturation process and partial diffusion process, i.e., a decrease in random coil structure by oligomerization of multiple partially unfolded monomers forming nuclei during the early nucleation phase of INS fibrillation. Furthermore, since the characteristic peak of β -sheet structure appears at 1615~1630 cm⁻¹,^{13, 22, 23} the change in the peak B intensity indicates a structural transition induced by diffusion and protein-protein collision process, i.e., an increase in β -sheet structure by protein-protein interaction leading to the formation of prefibrils and fibrils. Figure S19 depicts the variation in the intensity, i.e., the ratio of two fitted peaks A and B. Their incubation time-dependences, i.e., the magnitudes of changes before and after fibril formation, are observed. This result indicates that the denaturation-controlled and diffusion-controlled processes are independent during the overall fibrillation process.

Since the INS diffusion coefficient (D_{INS}) is smaller in D₂O than that in H₂O (viscosity of D₂O > viscosity of H₂O), the fibril elongation rates of INS in ordinary water and heavy water would be notably different from each other if the fibrillation is a diffusion-controlled process. However, our results of ThT assay using fully denatured INS and IR spectroscopy suggest that the fibrillation kinetics of INS in both ordinary and heavy water under our experimental conditions (H₂O at pH = 2.1, D₂O at pH = 2.1, 50 °C, 1-17 mg/ml INS) are dominantly affected by the rate of structural transition from native INS in either monomer or dimer form to partially unfolded INS, i.e., denaturation-controlled process.

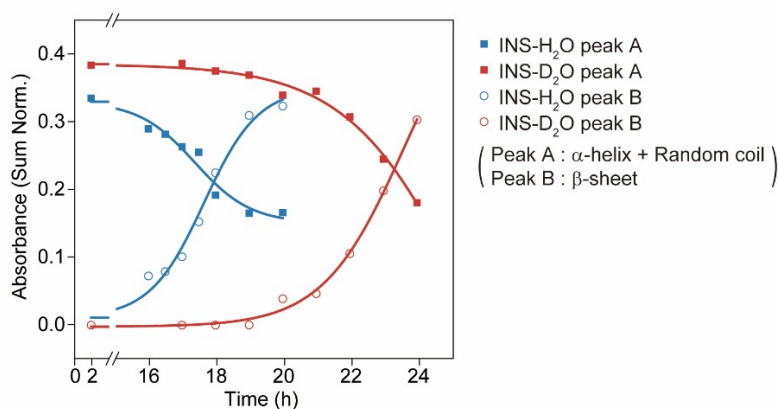


Figure S19 Intensity analysis of two peaks in linear IR spectra (Figure 2). The variation of peak A indicates a structural transition by denaturation process and partial diffusion process. The variation of peak B indicates a structural transition by the diffusion process.

Additional Supplementary Figure

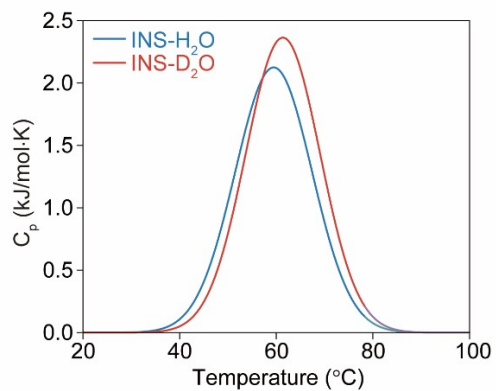


Figure S20 DSC thermograms of INS- H_2O (blue) and INS- D_2O (red). The transition (unfolding) enthalpy (ΔH_u) is the area under the curve, and the thermal transition midpoint (T_0) is the temperature where the heat capacity (C_p) is maximum.

Supplementary References

1. P. K. Glasoe and F. A. Long, *J. Phys. Chem.*, 1960, **64**, 188-190.
2. N. Mora-Diez, Y. Egorova, H. Plommer and P. R. Tremaine, *RSC Adv.*, 2015, **5**, 9097-9109.
3. L. E. Hokin, P. Sastry, P. R. Galsworthy and A. Yoda, *PNAS*, 1965, **54**, 177.
4. D. K. Nordstrom, C. N. Alpers, C. J. Ptacek and D. W. Blowes, *Environ. Sci. Technol.*, 2000, **34**, 254-258.
5. D. Perrin, *Buffers for pH and Metal Ion Control*, Springer Science & Business Media, 2012.
6. A. Micsonai, F. Wien, É. Bulyáki, J. Kun, É. Moussong, Y.-H. Lee, Y. Goto, M. Réfrégiers and J. Kardos, *Nucleic Acids Res.*, 2018, **46**, W315-W322.
7. E. Lindahl, B. Hess and D. Van Der Spoel, *J. Mol. Model.*, 2001, **7**, 306-317.
8. S. Pronk, S. Páll, R. Schulz, P. Larsson, P. Bjelkmar, R. Apostolov, M. R. Shirts, J. C. Smith, P. M. Kasson, D. Van Der Spoel, B. Hess and E. Lindahl, *Bioinformatics*, 2013, **29**, 845-854.
9. D. Van Der Spoel, E. Lindahl, B. Hess, G. Groenhof, A. E. Mark and H. J. C. Berendsen, *J. Comput. Chem.*, 2005, **26**, 1701-1718.
10. J. R. Grigera, *J. Chem. Phys.*, 2001, **114**, 8064-8067.
11. D. Svergun, C. Barberato and M. H. J. Koch, *J. Appl. Crystallogr.*, 1995, **28**, 768-773.
12. D. H. A. Corrêa and C. H. I. Ramos, *Afr. J. Biochem. Res.*, 2009, **3**, 164-173.
13. M. Bouchard, J. Zurdo, E. J. Nettleton, C. M. Dobson and C. V. Robinson, *Protein Sci.*, 2000, **9**, 1960-1967.
14. B. W. Chelgren and T. P. Creamer, *J. Am. Chem. Soc.*, 2004, **126**, 14734-14735.
15. Y. Marcus and A. Ben-Naim, *J. Chem. Phys.*, 1985, **83**, 4744-4759.
16. G. C. Kresheck, H. Schneider and H. A. Scheraga, *J. Phys. Chem.*, 1965, **69**, 3132-3144.
17. S.-Y. Sheu, E. W. Schlag, H. Selzle and D.-Y. Yang, *J. Phys. Chem. A*, 2008, **112**, 797-802.
18. K. B. Shelimov, D. E. Clemmer, R. R. Hudgins and M. F. Jarrold, *J. Am. Chem. Soc.*, 1997, **119**, 2240-2248.
19. S. J. Valentine, A. E. Counterman and D. E. Clemmer, *J. Am. Soc. Mass Spectrom.*, 1997, **8**, 954-961.
20. S. J. Valentine, J. G. Anderson, A. D. Ellington and D. E. Clemmer, *J. Phys. Chem. B*, 1997, **101**, 3891-3900.
21. W. Xiong, D. B. Strasfeld, S.-H. Shim and M. T. Zanni, *Vib. Spectrosc.*, 2009, **50**, 136-142.
22. L. N. Garriques, S. Frokjaer, J. F. Carpenter and J. Brange, *J. Pharm. Sci.*, 2002, **91**, 2473-2480.
23. F. Piccirilli, S. Mangialardo, P. Postorino, L. Baldassarre, S. Lupi and A. Perucchi, *Soft Matter*, 2012, **8**, 11863-11870.